Food Bioprocess Technol (2015) 8:1126–1138
DOI 10.1007/s11947-015-1477-0

ORIGINAL PAPER

Nondestructive Detection of Soluble Solids Content of Apples from Dielectric Spectra with ANN and Chemometric Methods

Wenchuan Guo · Liang Shang · Xinhua Zhu · Stuart O. Nelson

Received: 6 January 2014 / Accepted: 19 January 2015 / Published online: 7 February 2015
© Springer Science+Business Media New York 2015

Abstract To investigate the feasibility of using dielectric spectra in nondestructively determining the soluble solids content (SSC) of fruits, the dielectric constants and loss factors of 160 apples of three varieties (Fuji, Red Rome, and Pink Lady) were obtained at 51 discrete frequencies from 10 to 1800 MHz with an open-ended coaxial-line probe and an impedance/material analyzer. Based on the joint *x*–*y* distances sample set partitioning (SPXY) method, 106 apples were selected for the calibration set and the other 54 samples were used for the prediction set. The principal component analysis (PCA), uninformative variables elimination method (UVE-PLS), based on partial least squares, and successive projection algorithm (SPA) were applied to extract characteristic variables from original full dielectric spectra. The generalized regression neural network (GRNN), support vector machine (SVM) and extreme learning machine (ELM) modeling methods were used to establish models to predict SSC of apples, based on the original full dielectric spectra and characteristic variables, respectively. Results showed that four principal components were selected as characteristic variables by PCA, 15 dielectric constants and 14 loss factors at different frequencies were selected as characteristic variables by UVE-PLS, and one dielectric constant and ten loss factors were chosen as feature variables by SPA. ELM combined with SPA had the best SSC prediction performance, with calibrated correlation coefficient and predicted correlation coefficient of 0.898 and 0.908, respectively, and calibrated root-mean-square error and predicted root-mean-square error of 0.840 and 0.822, respectively. The study indicates that dielectric spectra combined with artificial neural network and chemometric methods might be applied in nondestructive determination of SSC of apples.

Keywords Apple · Dielectric properties · Soluble solids content · Generalized regression neural network · Support vector machine · Extreme learning machine

Data obtained by Wenchuan Guo as a visiting scholar at the Russell Research Center, USDA, ARS, Athens, Georgia, USA.

W. Guo (✉) · L. Shang · X. Zhu
College of Mechanical and Electronic Engineering, Northwest A&F University, Yangling, Shaanxi 712100, China
e-mail: guowenchuan69@126.com

W. Guo
e-mail: wencg915@sina.com

S. O. Nelson
Russell Research Center, US Department of Agriculture, Agricultural Research Service, Athens, GA 30605, USA

Introduction

Fruit is a major agricultural product in the world. It is usually sorted on the basis of size, shape, color, and surface defects. However, internal qualities, i.e., sweetness, acidity, and firmness, determine whether a fruit is appealing to customers. Sweetness is the main attribute of fruit internal qualities. It is usually determined by soluble solids content (SSC), which is mostly sugars (i.e., 80–85 %), and therefore a measure of sweetness (Guo et al. 2007a, b). Traditionally, SSC is measured with an Abbe refractometer or digital refractometer on juice extracted from the fruit. The major shortcoming of this method is its destructive nature. To realize fruit grading according to internal qualities, methods must be found for nondestructively predicting internal qualities.

Dielectric properties of materials are those electrical properties that determine the interaction of the material with electric fields. These properties can be defined in terms of the complex relative permittivity, $\varepsilon=\varepsilon'+j\varepsilon''$, where ε', the real part, is the dielectric constant and ε'', the imaginary part, is

the dielectric loss factor. The dielectric constant is associated with the capability of energy storage in the material, and the loss factor is associated with energy dissipation in the material in the form of heat. Since the first data on dielectric properties of grain were published (Nelson et al. 1953), more and more research has been undertaken on dielectric properties of agriculture products and food materials. Research has demonstrated that the dielectric properties of food materials are related to their composition, including such constituents as water (Feng et al. 2002), ash (Luczycka et al. 2013), and salt (Huang et al. 2013b). In studying the relationship between dielectric properties and internal qualities of honeydew melons, a close linear correlation was found between the dielectric properties and SSC in the complex plane of ε'/SSC and ε''/SSC (Nelson et al. 2006). However, the SSC could not be predicted well from the linear regression model (Guo et al. 2008). Other efforts have also been devoted to studying the linear correlation between dielectric properties and SSC in either external surface measurements or internal tissue measurements in several kinds of fruits, such as apples (Guo et al. 2011), watermelons (Nelson et al. 2007), and peaches (Guo and Chen 2010), but no obvious linear relationships were noted. Nonlinear models to predict internal qualities of fruits from dielectric spectra need to be explored and evaluated.

Artificial neural network (ANN) analysis is an effective nonlinear modeling method. It is useful in expressing complex relationships between different variables with nonlinear models. ANN methods have been used widely in pattern recognition (Ghiasabadi et al. 2013; Masood and Hassan 2013) and signal processing (Qian et al. 2013; Zhang et al. 2013a, b; Zhu et al. 2013). However, the precision of ANN models is usually influenced by data overlap and noise. To overcome this problem, chemometric methods are often used to extract indispensable information from large sets of original data. Several studies have shown that the SSC of fruits could be predicted well from their visible/near infrared (Vis/NIR) spectra when combined ANN and chemometric methods are applied (Liu et al. 2010, 2012; Peng and Lu 2008; Moller et al. 2013; Li et al. 2013; Jie et al. 2013; Jiang and Zhu 2013). However, to our knowledge, no attempt has been made to predict SSC of fruits from their dielectric spectra with ANN and chemometric methods. Therefore, the dielectric spectra of three varieties of apples (Fuji, Red Rome, and Pink Lady) were obtained over the frequency range from 10 to 1800 MHz, and chemometric methods, such as principal component analysis (PCA), uninformative variables elimination, based on partial least squares (UVE-PLS), and successive projection algorithm (SPA), were applied to extract characteristic variables from original full dielectric spectra. Several ANN modeling models, such as generalized regression neural network (GRNN), support vector machine (SVM), and extreme learning machine (ELM), were used to establish nonlinear models to predict soluble solids content of apples. The performance of different ANN models on determination of SSC in apples was compared when full spectra, selected characteristic variables by PCA, UVE-PLS, and SPA were used as inputs. The feasibility of using dielectric spectra for nondestructive determination of SSC in apples of three varieties is discussed.

Materials and Methods

Apples

Fresh apples of three varieties, ‘Fuji’, ‘Pink Lady’, and ‘Red Rome’, were obtained from refrigerated apple storage rooms in north Georgia within 2 weeks of harvest for the study. Measurements were taken initially and at 2-week intervals during 10 weeks of storage. At each measurement time, ten apples of each variety were measured. Totally, 160 apples were used in the work, including 60 ‘Fuji’, 60 ‘Pink Lady’, and 40 ‘Red Rome’ apples. The detailed information on apple samples was described previously (Guo et al. 2007a, b).

Dielectric Properties Measurement and Experimental Procedures

The dielectric properties measurement system consisted of a Hewlett-Packard 4291A impedance/material analyzer, a Hewlett-Packard (Palo Alto, CA) 85070B open-ended coaxial-line probe, a computer, and a laboratory jack. The permittivities (ε' and ε'') were calculated with Agilent Technologies 85070D dielectric probe kit software from the reflection coefficient of the material in contact with the active tip of the coaxial-line probe. The measurement was set at 51 discrete frequencies on a logarithmic scale from 10 to 1800 MHz. The schematic diagram of the dielectric properties measurement system is shown in Fig. 1.

The permittivity measurements of intact apples were made with the probe in firm contact with the surface of the apples in the equatorial region at four points about 90° apart around the perimeter of the fruit. The SSC of juice expressed from the apple tissue was determined with an Atago Pallete Series Model PR101 digital refractometer (Atago Co. Ltd., Tokyo,

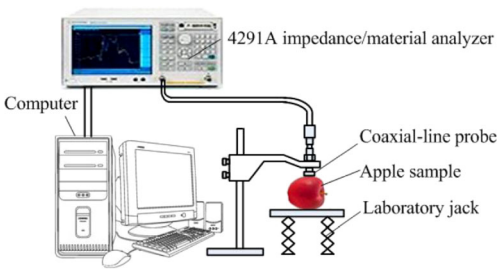

Fig. 1 The schematic diagram of the dielectric properties measurement system

Japan). Three SSC readings were taken for each apple. Averages of the four permittivity measurements and three SSC readings for each apple were used. All experiments were done at room temperature (24±1 °C). The detailed calibrations for the impedance/material analyzer and open-ended coaxial-line probe and experimental procedures were described previously (Guo et al. 2007a, b).

Dielectric Spectra

Each sample had two dielectric spectra, dielectric constant spectrum and loss factor spectrum. Each spectrum was made up of 51 values at different frequencies. Thus, the dielectric properties collected for each sample (apple) consisted of 102 values. From 10 to 1800 MHz, each value was numbered. The obtained dielectric constants were numbered 1–51, and the loss factors were numbered 52–102. So, the permittivity data for each sample was a 102-dimensional vector.

Sample Division Method

Effective and rational division of the sample set is essential for establishing models, and it always has direct influence on prediction accuracy. Sample set partitioning based on joint *x*–*y* distances (SPXY) is an algorithm evolved from Kennard Stone to divide calibration set and prediction set (Galvao et al. 2005). Some studies have shown that SPXY can improve predictive performance (Zhan et al. 2009). In SPXY, the distance of variables *x* and *y* is considered simultaneously so that a more reasonable calibration set and prediction set can be acquired.

Euclidean distance $d_x(p,q)$ can be calculated as:

$$d_x(p,q) = \sqrt{\sum_{j=1}^{J} \left[x_p(j) - x_q(j)\right]^2}; \quad p,q \in [1,N] \tag{1}$$

where $x_p(j)$ and $x_q(j)$ are the instrumental response at the *j*-th variable of samples *p* and *q*, respectively. *J* refers to the number of all variables, and *N* refers to the number of all samples. In this study, *J* and *N* are 102 and 160, respectively.

The value $d_y(p,q)$ can be calculated as follows:

$$d_y(p,q) = \sqrt{\left(y_p - y_q\right)^2} = \left|y_p - y_q\right|; \quad p,q \in [1,N] \tag{2}$$

where y_p and y_q are target attributes of samples *p* and *q*, respectively.

The value $d_{xy}(p,q)$ can be calculated as:

$$d_{xy}(p,q) = \frac{d_x(p,q)}{\max_{p,q\in[1,N]} d_x(p,q)} + \frac{d_y(p,q)}{\max_{p,q\in[1,N]} d_y(p,q)}; \quad p,q \in [1,N] \tag{3}$$

Based on $d_{xy}(p,q)$, samples in the calibration set can be selected to establish models. Remaining samples were used for the prediction set to validate the established model.

Characteristic Variables Selection Methods

To reduce the effect of noise, ignore reduplicative message, and simplify models, it is necessary to obtain characteristic or primary variables from full frequencies of dielectric spectra (FF).

Principal Component Analysis

PCA is a conventional information concentrating method. It is usually used to simplify data by reducing the number of variables into a smaller number of orthogonal variables. It is also the most optimal method to seek a linear combination of the principal components (PCs) from original variables. PCA can explain the data structure characteristics without losing original information. PCs are usually ordered from large to small based on the contribution rate of each PC. The PCs listed in front show more variance among the data, and the last few PCs, which have lesser variance, are usually ignored because they may have a noise effect (Nashat and Abdullah 2010).

Uninformative Variables Elimination Method Based on Partial Least Squares

UVE-PLS is an effective pretreatment method based on regression coefficient of partial least squares (PLS) to select characteristic variables. It has been widely applied in Vis/NIR spectra (Jie et al. 2013; Wu et al. 2013). A stability value *C* and *cutoff* threshold are implemented to evaluate the dependability of each variable. *C* is defined as:

$$C_i = \frac{\text{mean}(b_i)}{\text{std}(b_i)}; \quad i = 1, \quad 2, \quad \ldots, \quad m \tag{4}$$

where b_i denotes the regression coefficient of the *i*-th variable in calibration samples. mean(b_i) and std(b_i) are the mean and standard deviation of b_i, respectively. *m* is the number of input variables. By adding artificial random samples, *cutoff* threshold is defined as:

$$cutoff = k \times \left|\max(C_{\text{random}})\right| \tag{5}$$

where *k* is the contribution coefficient and max(C_{random}) expresses the maximum *C* of artificial random samples. The dimension and quantity of artificial random samples are the same as those for the calibration samples. Characteristic variables were selected according to stability value of each variable and *cutoff* threshold (Deng et al. 2013; Huang et al. 2013c). More details on the UVE-PLS process can be found elsewhere (Centner et al. 1996).

Successive Projection Algorithm

SPA is a forward-loop variable selection method. Based on convex geometry and orthogonal projection, it can select some characteristic variables to replace all variables (Zhang et al. 2008). Moreover, complexity of the model and linear correlation effects between different variables can be reduced effectively by SPA. After a variable is chosen, another new variable is added each time until the preset variable number is reached. This method has been widely used in Vis/NIR spectra preprocessing and has provided good performance (Pontes et al. 2005; Ye et al. 2008).

Modeling Methods

Generalized Regression Neural Network

GRNN is a kind of radial basis function network. This neural network consists of four layers: input, pattern, summation, and output layers. In GRNN modeling, the estimated $\hat{Y}(x)$, which represents a weighted term for all observed values Y_i, can be calculated as (Specht 1991):

$$\widehat{Y}(x) = \frac{\sum_{i=1}^{N} Y_i \exp\left(-\frac{D_i}{2\sigma^2}\right)}{\sum_{i=1}^{N} \exp\left(-\frac{D_i}{2\sigma^2}\right)} \tag{6}$$

where Y_i expresses the i-th observed value, N is the sample size, and σ is the wide spread coefficient of the Gaussian function, also called the smoothing factor. D_i is defined as

$$D_i = \sqrt{(x-x_i)^{\mathrm{T}}(x-x_i)} \tag{7}$$

where x is the observed input value and x_i is the i-th neuron of the corresponding sample. Equation 6 indicates that the smoothing factor is the primary parameter of the GRNN.

Support Vector Machine

SVM is a machine learning method based on statistical learning theory (Burges 1998). The main idea for SVM is to build a hyperplane as a decision surface, which makes the positive-examples and counter-examples have the largest distance. SVM employs a set of linear equations instead of quadratic programming problems to obtain the support vectors, and it embodies the structural risk minimization principle instead of the traditional empirical risk minimization principle to avoid overfitting problems. It is useful in studying high-dimensional features with fewer training data. SVM has been extensively used in image processing (Liu and Li 2013) and in nondestructive evaluation (Deng et al. 2013). The SVM regression model can be defined as follows (Cherkassky and Ma 2004):

$$f(x) = \sum_{i=1}^{N} \alpha_i K(x, x_i) + b \tag{8}$$

where N is the number of input vectors, α_i is the i-th Lagrange multiplier, x_i is the i-th input vector, $K(x,x_i)$ is the kernel function, and b is the bias. $K(x,x_i)$ is a symmetric function that must follow Mercer's condition. Compared with a linear kernel and other nonlinear kernels, a radial basis function (RBF) kernel can deal with the nonlinear relationship between input vectors and target attributes. So RBF was used as the kernel function in this study. RBF is defined as:

$$K(x, x_i) = \exp\left(-\|x-x_i\|^2 \Big/ \left(2g^2\right)\right) \tag{9}$$

where $\|x-x_i\|$ is the distance between the i-th input vector and threshold vector, and g is the width vector.

Compared with other machine learning methods, SVM shows superiority in generalization and prediction. In this study, SVM models were established by Matlab 7.14.0.739 (R2012a; Math Works, Massachusetts, USA) and Libsvm tool box (http://www.csie.ntu.edu.tw/~cjlin/). Detailed information on SVM can be found elsewhere (Collobert and Bengio 2001; Furey et al. 2000).

Extreme Learning Machine

ELM is a new efficient single-hidden-layer feed-forward neural network with good generalization performance. Its computational process can be listed as follows.

Step 1. Given a training set L, number of input nodes N and number of hidden-layer neurons $\widehat{N}$. L is defined as $L=\{(\mathbf{x}_j,\mathbf{t}_j)|\mathbf{x}_j\in\mathbf{R}^n,\mathbf{t}_j\in\mathbf{R}^m,j=1,2,\ldots,N\}$, where $\mathbf{x}_j$ is the j-th input vector ($n\times1$) and $\mathbf{t}_j$ is the j-th target vector ($m\times1$).

Then assign parameters $\mathbf{w}_i$ and b_i (i=1, 2, … $\widehat{N}$) randomly. $\mathbf{w}_i$ is the weight vector which connects input neuron nodes and the i-th hidden node. b_i is a threshold value of the i-th hidden node.

Step 2. Select an excitation function $g(x)$. Calculate the output matrix of the hidden layer H as

$$\mathrm{H}\left(\mathbf{w}_1,\ldots,\mathbf{w}_{\widehat{N}},b_1,\ldots,b_{\widehat{N}},\mathbf{x}_1,\ldots,\mathbf{x}_N\right) = \begin{bmatrix} g(\mathbf{w}_1\cdot\mathbf{x}_1+b_1) & \cdots & g\left(\mathbf{w}_{\widehat{N}}\cdot\mathbf{x}_1+b_{\widehat{N}}\right) \\ \vdots & \cdots & \vdots \\ g(\mathbf{w}_1\cdot\mathbf{x}_N+b_1) & \cdots & g\left(\mathbf{w}_{\widehat{N}}\cdot\mathbf{x}_N+b_{\widehat{N}}\right) \end{bmatrix}_{N\times\widehat{N}} \tag{10}$$

Step 3. Calculate the weight matrix of output by $\boldsymbol{\beta} = \mathbf{H}^{\dagger}\mathbf{T}$. $\mathbf{H}^{\dagger}$ is the Moore–Penrose generalized inverse of $\mathbf{H}$, and $\mathbf{T}$ is the target matrix. Matrix $\boldsymbol{\beta}$ and matrix $\mathbf{T}$ can be calculated by

$$\boldsymbol{\beta} = \begin{bmatrix} \boldsymbol{\beta}_1^{\mathrm{T}} \\ \vdots \\ \boldsymbol{\beta}_{\overline{N}}^{\mathrm{T}} \end{bmatrix}_{\overline{N}\times m} \quad \text{and} \quad \mathbf{T} = \begin{bmatrix} \mathrm{t}_1^{\mathrm{T}} \\ \vdots \\ \mathrm{t}_N^{\mathrm{T}} \end{bmatrix}_{N\times m} \tag{11}$$

where $\boldsymbol{\beta}_i$ is a link weight of the i-th hidden node. More detailed processing of ELM can be found in other publications (Huang et al. 2006; Liu and Wang 2013).

Evaluation of Model Performance

Model performance of calibration and prediction is always evaluated by the root-mean-square error of calibration (RMSEC), root-mean-square error of prediction (RMSEP), correlation coefficient of calibration (R_c), and correlation coefficient of prediction (R_p). These indices are defined as

$$R_c = \sqrt{\sum_{i=1}^{n_c}\left(\hat{y}_i - y_i\right)^2} \Big/ \sqrt{\sum_{i=1}^{n_c}\left(\hat{y}_i - y_{mc}\right)^2} \tag{12}$$

$$R_p = \sqrt{\sum_{j=1}^{n_p}\left(\hat{y}_j - y_j\right)^2} \Big/ \sqrt{\sum_{j=1}^{n_p}\left(\hat{y}_j - y_{mp}\right)^2} \tag{13}$$

$$\mathrm{RMSEC} = \sqrt{\frac{1}{n_c}\sum_{i=1}^{n_c}\left(\hat{y}_i - y_i\right)^2} \tag{14}$$

$$\mathrm{RMSEP} = \sqrt{\frac{1}{n_p}\sum_{j=1}^{n_p}\left(\hat{y}_j - y_j\right)^2} \tag{15}$$

where $\hat{y}_i$ and y_i are the predicted value and the measured value of the i-th sample in the calibration set, respectively; $\hat{y}_j$ and y_j are the predicted value and the measured one of the j-th sample in the prediction set, respectively; y_{mc} and y_{mp} are the mean values of the samples in the calibration set and the prediction set, respectively; n_c and n_p are the numbers of samples in the calibration set and the prediction set, respectively (Liu et al. 2010). Usually, a model with higher R_c and R_p and lower RMSEC and RMSEP is stable and works well (Li et al. 2013).

Results and Discussion

Dielectric Spectra of Apples

The averages with the standard deviations of the dielectric constants and loss factors of the three cultivars of apples over the frequency range from 10 to 1800 MHz are shown in Fig. 2. The dependence of ε' and ε'' on frequency is similar for the three cultivars. The ε' value decreased with increasing frequency over the entire frequency range. However, an overriding dielectric relaxation behavior was observed for ε''. The behavior may involve bound water and Maxwell–Wagner relaxations (Guo et al. 2007a, b). Figure 2 also shows that when the frequency increased from 10 to 1800 MHz, the decrease of ε' for 'Fuji' apples was the smallest, which decreased from 40.27 to 21.88, while the decrease was largest for 'Pink Lady' apples, from 42.74 to 20.22. The ε'' of 'Pink Lady' apples was larger than that of 'Fuji' and 'Red Rome' over the whole investigated frequency range. An obvious overlap of ε'' of 'Fuji' and 'Red Rome' apples was noted between 30 and 300 MHz. It was also noticed that both for dielectric constant and loss factor, the standard deviations decreased with increasing frequency.

Division of Samples into Calibration and Prediction Sets

One hundred sixty apples were divided into calibration and prediction sets according to SSC with the SPXY procedure. The ratio of samples in the calibration and prediction sets was 2:1. The calibration set consisted of 40 'Fuji', 40 'Pink Lady', and 26 'Red Rome' apples, and the prediction set had 20 'Fuji', 20 'Pink Lady', and 14 'Red Rome' apples. The statistics for the SSC values for calibration and prediction sets are shown in Table 1. Also, the results of the analysis of variance (ANOVA) on SSC of the three varieties of apples are listed. The results showed that not only in the calibration set but also in the prediction set the SSC values of the three varieties had significant differences at the probability level of 5 %. Table 1 also shows that the range of SSC of each variety in the calibration set was larger than that in the prediction set, indicating the sample division into the calibration and prediction sets was reasonable.

Selection of Characteristic Variables

Selection of Characteristic Variables by PCA

Table 2 lists the accumulative contribution rates of the first seven PCs. It indicates that the contribution rate of the first principal component (PC1) was 99.588 %, which offers the main contribution, and the accumulative contribution rate of the first seven PCs came to 99.999 %. Because more variables were used in establishing the model, it causes the model be

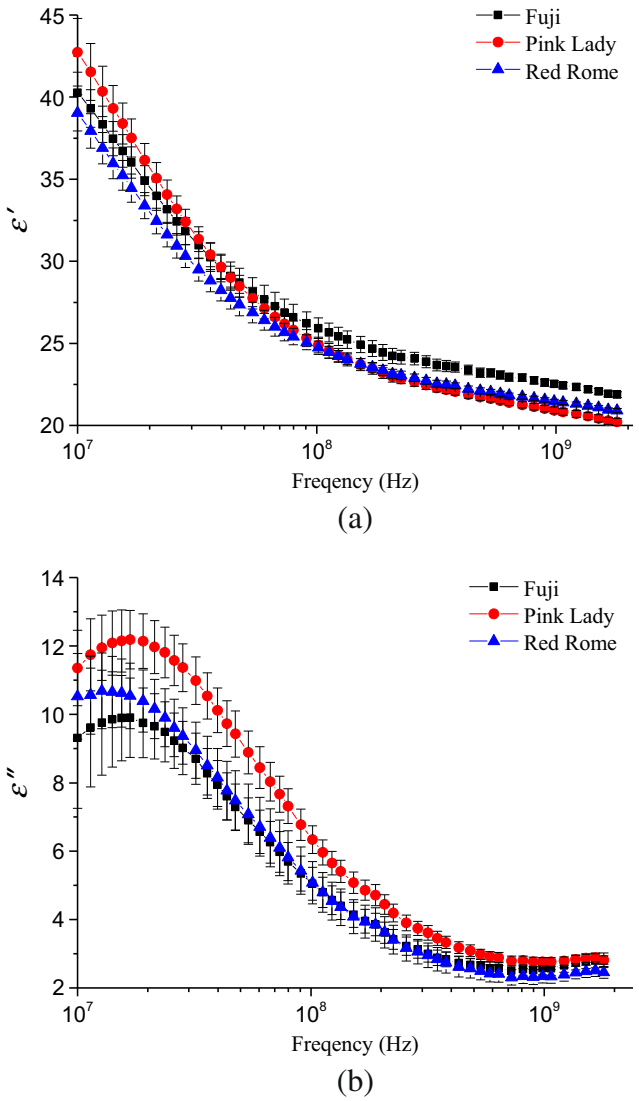

Fig. 2 Frequency dependence of ε' (**a**) and ε'' (**b**) of three different varieties of apples

more complicated. In this work, the least amount of PCs was applied in modeling when the accumulative contribution rate was higher than 99.990 %. Finally, the first four PCs, whose accumulative rate could explain 99.994 % of the total variance scores, were adopted in the study and were considered as the inputs of the GRNN, SVM, and ELM models.

Selection of Characteristic Variables by UVE-PLS

UVE-PLS process is influenced by some underlying variables of PLS, which are usually called latent variables (Wold et al. 2001). However, the number of latent variables is not known usually. Therefore, different numbers of latent variables were used as the inputs of PLS to establish the UVE-PLS model to eliminate uninformative variables from the dielectric spectra of dielectric constant and loss factor. The numbers of eliminated uninformative variables are often different when different latent variables are used in UVE-PLS. A previous study showed that the number of latent variables was between 1 and 15 in the study. Therefore, the number of latent variables used as the input of the PLS was set from 1 to 15, and the best number of latent variables was determined according to the smallest RMSEC. The changed RMSEC with the number of latent variables is shown in Fig. 3. It shows that when the number of latent variables was 9, the RMSEC was the smallest (0.847). So, the optimal number of latent variables was 9 in this study. More information about latent variables can be found elsewhere (Wold et al. 2001).

In the UVE-PLS process, the calculated contribution coefficient k in Eq. (5) was 0.99. According to the stability value C of random variables in Eq. (4), the *cutoff* threshold in Eq. (5) was calculated as 15.84. Figure 4 shows the stability of each variable in the dielectric spectra for apple SSC prediction by UVE-PLS with nine latent variables. The input dielectric variables were at the left of the vertical line, while random variables were at the right side. The *cutoff* threshold of UVE-PLS is indicated by dashed lines. The dielectric variables whose stability is within the *cutoff* lines should be treated as uninformative and eliminated. Finally, 29 dielectric variables, including 15 for ε' and 14 for ε'', were selected by UVE-PLS from the full dielectric spectra of ε' and ε''. The number of selected dielectric variables was 28.4 % of the 102 variables in the full spectra. Figure 5 shows the 29 dielectric variables selected by UVE-PLS. The curves show the original dielectric spectra of one sample in the calibration set, and the vertical lines represent selected variables. The selected variables were used to establish ANN models.

Table 1 Statistics for the SSC values of apple samples determined by SPXY

Samples	Calibration set				Prediction set			
	Num	Max/°Bx	Min/°Bx	Mean±SD/°Bx	Num	Max/°Bx	Min/°Bx	Mean±SD/°Bx
Fuji	40	21.6	14.5	18.2±1.4 a	20	20.3	16.9	18.5±1.2 a
Pink	40	16.3	13.9	15.2±0.6 b	20	16.2	14.3	15.2±0.5 b
Rome	26	16.5	13.1	14.6±0.9 c	14	15.6	13.1	14.5±0.7 c

A column followed by different letters are significantly different at 5 % probability level

SD standardized form

Table 2 The contribution rates and accumulative contribution rates of the first seven PCs

The number of principal components	PC1	PC2	PC3	PC4	PC5	PC6	PC7
Contribution rate (%)	99.588	0.314	0.081	0.011	0.003	0.001	0.001
Accumulative contribution rate (%)	99.588	99.902	99.983	99.994	99.997	99.998	99.999

Selection of Characteristic Variables by SPA

The characteristic variables selection process by SPA was implemented by comparing the RMSEC values under different variable numbers from 1 to 25. Figure 6 shows that the RMSEC decreased with the increase of number of variables. When the RMSEC did not decrease significantly, the number of variables could be determined. In this study, 11 characteristic variables were determined. At this point, RMSEC= 0.850. The characteristic variables selected by SPA are shown in Table 3. One ε' variable and 10 ε'' variables at different frequencies were selected as characteristic variables. The number of selected dielectric variables was 10.8 % of the 102 variables in the full spectra.

SSC Determination Models

SSC Determination Models Developed by GRNN

The best smoothing factor (σ) for GRNN in Eq. (6) was confirmed by modeling repeatedly when σ was set from 0.1 to 2. In this study, smoothing factors of FF, PCA, UVE-PLS, and SPA were 0.5, 0.1, 0.2, and 0.2, respectively (Table 4). This indicates that at these smoothing factors, the performances of networks were best.

Table 5 shows the calibration and prediction performances of the GRNN models developed for determining apple SSC when FF, selected characteristic variables by PCA, UVE-PLS, and SPA were used in modeling, respectively. The results show that when the selected 29 characteristic variables by UVE-PLS were used as input data, the GRNN-UVE-PLS model had the highest R_c (0.952) and R_p (0.880) and the smallest RMSEC (0.565) and RMSEP (1.243). This means that the calibration and prediction ability of the GRNN-UVE-PLS was the best. The GRNN model based on PCA had the lowest R_c (0.899) and a higher RMSEC (0.807), but a better prediction ability with R_p of 0.860 and RMSEP of 1.358. Although GRNN-SPA model had higher R_c (0.902) and R_p (0.867), it had the highest RMSEC and RMSEP. That is GRNN-SPA had the highest calibration and prediction errors. GRNN-FF model, which had a higher R_c (0.916) and a lower RMSEC (0.807), had the lowest R_p (0.839) and higher RMSEP (1.428). That means that the stability of GRNN-FF was not good. Moreover, all 102 variables used in the GRNN-FF model cause the model to be more complicated than the others.

SSC Determination Models Developed by SVM

Kernel function and optimal model parameters are first needed before developing the SVM calibration models. Since RBF can deal with nonlinear relationships between frequency spectra and target variables better than other functions, RBF was used as the kernel function for SVM in this study. Several studies have shown that the penalty factor *c*, which is a key

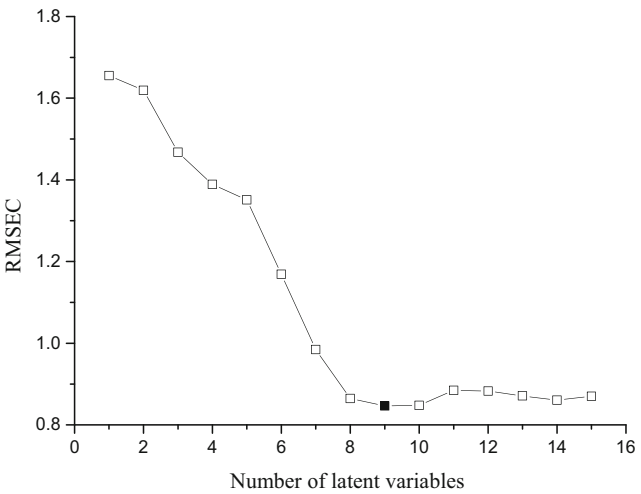

Fig. 3 Changed RMSEC with number of latent variables in UVE-PLS. *Filled square* represents the point at which the number of latent variables was finally selected

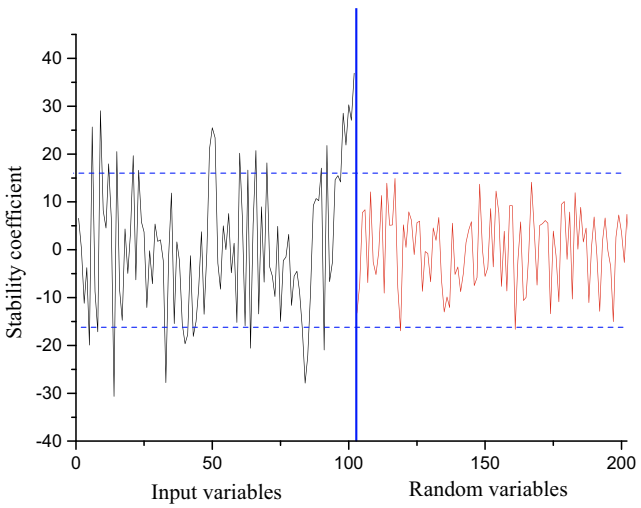

Fig. 4 Stability of each dielectric variable in the dielectric spectra for apple SSC predication by UVE-PLS with nine latent variables. Two *horizontal dashed lines* show the lower and upper cutoff

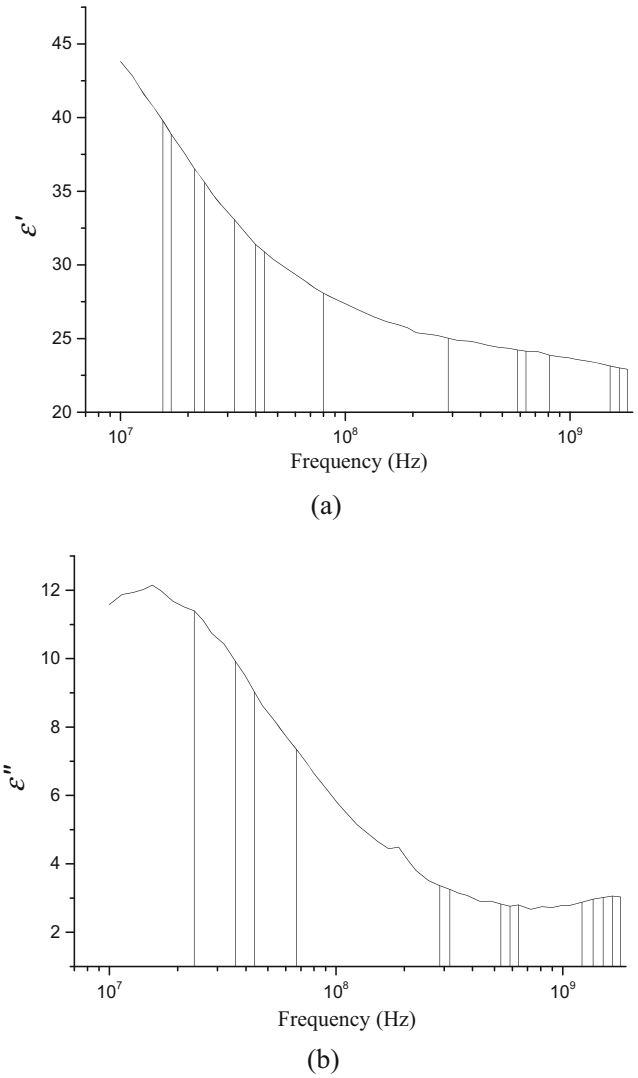

Fig. 5 Plots of selected 29 dielectric variables, including 15 dielectric constants (**a**) and 14 loss factors (**b**). Curves show the original dielectric spectra of sample one in calibration set. *Vertical lines* represent selected variables

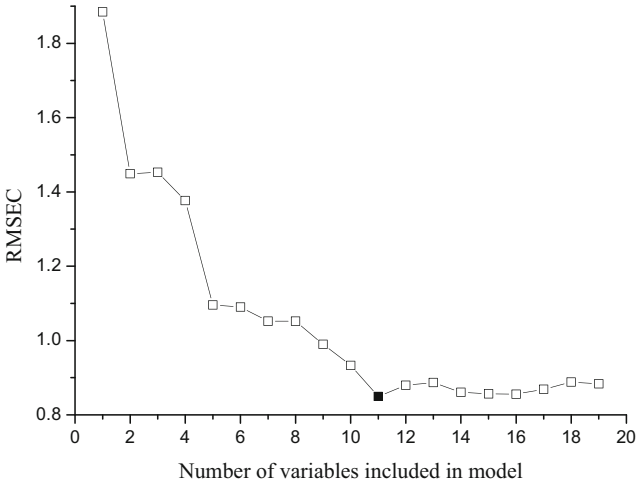

Fig. 6 Changed RMSEC with the number of variables included in SPA. *Filled square* represents the point at which the final number of variables was selected

regularization parameter of the SVM model, and parameter g of the RBF in Eq. (9) play essential roles in establishing SVM models. Detailed information about c can be found elsewhere (Cherkassky and Ma 2004).

In this study, fivefold cross-validation was applied to select c (range set from 2^{-6} to 2^{6}) and g (range set from 2^{-6} to 2^{6}) with an increment of $2^{0.5}$ for the SVM. Grid-Search method was employed to search for the optimal parameters. For each combination of c and g, SVM model was established and the RMSEC was calculated. The best values of c and g were determined by the smallest RMSEC in all combinations of c and g. Detailed processing for parameter selection is discussed elsewhere (Chang and Lin 2011; Cheng et al. 2013). Figure 7 summarizes the process of selecting parameters. The determined values of c and g at different variable selection methods are listed in Table 4.

The calibration and prediction performances of developed SVM models for determining apple SSC when FF, selected characteristic variables by PCA, UVE-PLS, and SPA were used in modeling are shown in Table 5. When the selected 11 characteristic variables by SPA were used to establish the SVM model, the SVM-SPA model had the highest R_c (0.926) and the lowest RMSEC (0.676) in the calibration set, but lower R_p (0.796) and higher RMSEP (1.684) in the prediction set. When the selected 29 characteristic variables selected by UVE-PLS were used as input data for SVM modeling, the SVM-UVE-PLS model had the highest R_p (0.871), lower RMSEP (1.484), higher R_c (0.907), and lower RMSEC (0.737). SVM-FF model had better calibration and prediction performances. SVM-PCA had the poorest SSC prediction performance among four SVM models since it had the lowest R_c (0.860) and R_p (0.775) and the highest RMSEC (0.939) and RMSEP (1.764). Generally, SVM-UVE-PLS has good potential in predicting SSC for apples in this study.

SSC Determination Models Developed by ELM

The excitation function of ELM was the "sig." function. The number of hidden layer nodes was obtained by a trial and error

Table 3 The 11 dielectric variables selected by SPA

Number	Frequency (MHz)	Dielectric properties	Number	Frequency (MHz)	Dielectric properties
1	32.099	ε'	7	585.501	ε''
2	19.097	ε''	8	897.380	ε''
3	23.674	ε''	9	1362.534	ε''
4	134.164	ε''	10	1654.179	ε''
5	430.659	ε''	11	1800.000	ε''
6	533.887	ε''			

Table 4 Modeling parameters of GRNN, SVM, and ELM

Pretreatment methods	GRNN	SVM		ELM		
	σ	c	g	Input layer nodes	Hidden layer nodes	Output layer nodes
FF	0.5	1	0.5	102	30	1
PCA	0.1	0.177	16	4	18	1
UVE-PLS	0.2	16	0.088	29	32	1
SPA	0.2	0.707	2.828	11	27	1

method. The methods is setting the number of hidden layer nodes from 1 to 100 at first, then increasing the number of hidden layer nodes by 1 from 1 gradually, next, deciding the optimal number of nodes based on the lowest RMSEP (Chen et al. 2012). Since the initial weight value of ELM was random, the modeling results were unstable. Therefore, a model repeated 1000 times was employed. According to the average results of RMSEP, the number of hidden layer nodes was decided reasonably. The average RMSEPs in 1000 times repetition under different numbers of hidden layer nodes for ELM with different characteristic variable selection methods of FF, PCA, UVE-PLS, and SPA are shown in Fig. 8. Based on the smallest RMSEP, the number of hidden layer nodes for ELM with FF, PCA, UVE-PLS, and SPA were 30, 18, 32, and 27, respectively. All determined parameters of the models under different characteristic variables selection methods are listed in Table 4.

The calibration and prediction performances of developed ELM models for determining apple SSC with different characteristic variables selection methods are summarized in Table 5. Table 5 shows that the model of ELM-UVE-PLS had the highest R_c (0.910), lowest RMSEC (0.789), higher R_p (0.860), and lower RMSEP (0.992). The ELM-SPA model had the highest R_p (0.908), the lowest RMSEP (0.822), and better calibration performance with R_c of 0.898 and RMSEC of 0.840. ELM-FF model had better calibration and prediction performances than that of ELM-PCA, which had the worst calibration and prediction performances among the four ELM models since it had the lowest R_c (0.747) and R_p (0.766) and the highest RMSEC (1.270) and RMSEP (1.248).

Comprehensive Comparison of SSC Determination Performance for Different Models

To determine the model with the best comprehensive performance for SSC determination, R_c+R_p, $|R_c-R_p|$, RMSEC+RMSEP, and response time, when a computer with the frequency of 1.8 GHz and internal memory of 4 GB was used, are also listed in Table 5. The model with the highest R_c+R_p, the smallest $|R_c-R_p|$ and RMSEC+RMSEP, and the least response time is regarded as the best one. Table 5 shows that GRNN-UVE-PLS had the highest R_c+R_p (1.832) among 12 models. However, it had higher $|R_c-R_p|$. It indicates that GRNN-UVE-PLS had bad stability. Moreover, its response time was higher (3.903 s). ELM-SPA had the smallest $|R_c-R_p|$ (0.010) and RMSEC+RMSEP (1.662). So, ELM-SPA was the most stable and had the lowest prediction error. Moreover, ELM-SPA had higher R_c+R_p (1.806) and less response

Table 5 Comparison of determination results for SSC of apples of three varieties by GRNN, SVM, and ELM models

Modeling method	Characteristic variables selection method	Calibration set		Predication set		R_c+R_p	$\lvert R_c-R_p\rvert$	RMSEC+RMSEP (°Bx)	Response time (s)
		R_c	RMSEC (°Bx)	R_p	RMSEP (°Bx)				
GRNN	FF	0.916	0.749	0.839	1.428	1.755	0.077	2.177	5.001
	PCA	0.899	0.807	0.860	1.358	1.759	0.039	2.165	2.012
	UVE-PLS	0.952	0.565	0.880	1.243	1.832	0.072	1.808	3.903
	SPA	0.902	0.841	0.867	1.529	1.769	0.035	2.370	2.589
SVM	FF	0.916	0.705	0.850	1.238	1.766	0.066	1.943	3.246
	PCA	0.860	0.939	0.775	1.764	1.635	0.085	2.703	2.167
	UVE-PLS	0.907	0.737	0.871	1.484	1.778	0.036	2.221	2.159
	SPA	0.926	0.676	0.796	1.684	1.722	0.130	2.360	1.670
ELM	FF	0.872	0.903	0.831	1.083	1.703	0.041	1.986	1.598
	PCA	0.747	1.270	0.766	1.248	1.513	0.019	2.518	1.298
	UVE-PLS	0.910	0.789	0.860	0.992	1.770	0.050	1.781	1.305
	SPA	0.898	0.840	0.908	0.822	1.806	0.010	1.662	1.396

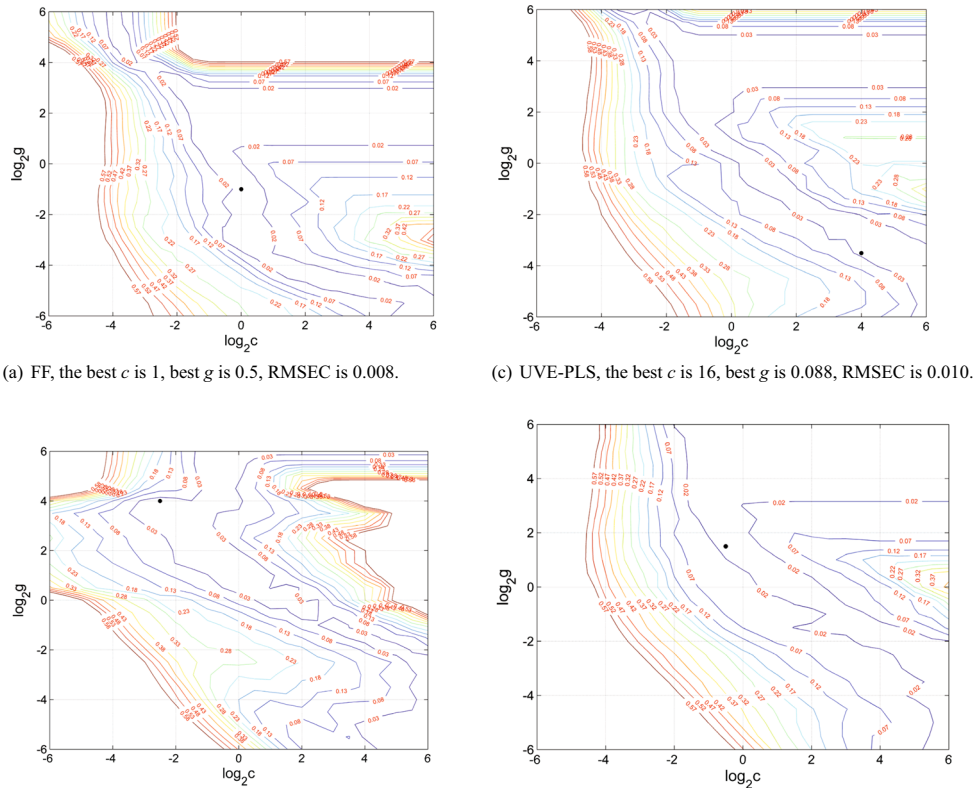

Fig. 7 The grid search process of penalty factor (c) and parameter g combination of three selection methods for SVM by fivefold cross validation. *Filled circle* indicates the optimal c and g for each model

(a) FF, the best c is 1, best g is 0.5, RMSEC is 0.008.

(c) UVE-PLS, the best c is 16, best g is 0.088, RMSEC is 0.010.

(b) PCA, the best c is 0.177, best g is 16, RMSEC is 0.026.

(d) SPA, the best c is 0.707, best g is 2.828, RMSEC is 0.008.

time (1.396). In addition, 11 variables used in ELM-SPA were less than the 29 variables used in GRNN-UVE-PLS. Therefore, the ELM-SPA model was regarded as the best in the determination of SSC of apples for the three varieties. The model was also found to be the best one in predicting SSC of pear by Fourier transform near infrared spectroscopy (Jiang and Zhu 2013). The calibration and prediction results for the ELM-SPA model are shown in Fig. 9.

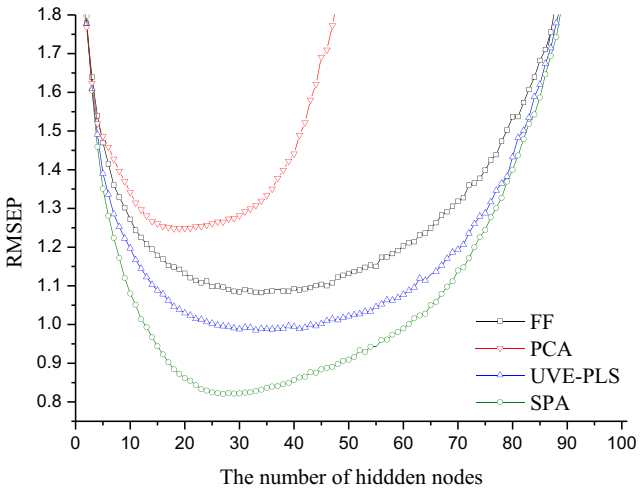

Fig. 8 The average RMSEP under different numbers of hidden layer nodes for ELM with characteristic variable selection methods of FF, PCA, UVE-PLS, and SPA

Investigating the process speed of all models, ELM, in contrast to GRNN and SVM, had less response time. That means that ELM can avoid some difficulties faced by gradient-based learning methods (Cao et al. 2012; Zhu et al. 2005). Furthermore, the stability of ELM was better than that of GRNN and ELM since most ELM models had lower $|R_c - R_p|$ than GRNN and SVM models.

Comparison with Reported Data

Vis/NIR spectroscopy technology or hyperspectral imaging technology combined with chemometric methods and ANN have been widely used to predict apple SSC. For example, based on Vis/NIR spectroscopy technology, SSC of 'Golden Delicious' and 'Stark Red Delicious' apples were predicted by PLS models with a correlation coefficient of cross-validation and root-mean-square error of 0.85 and 0.78, and 0.82 and 0.12, respectively (Beghi et al. 2013). PLS models were also built to predict SSC of 'Red Fuji' (Fan et al. 2009), 'Golden Delicious' (Giovanelli et al. 2014), and 'Elshof' (Moller et al. 2013) apples with R_p^2 and RMSEP of 0.98 and 0.29, 0.89 and 0.40, and 0.80 and 0.70, respectively. By using hyperspectral imaging technology, multiple linear regression models were built for 'Fuji' apples with R_p^2 and RMSEP of 0.95 and 0.31 (Huang et al. 2013a) and for 'Golden Delicious' apples with R_p of 0.88 (Peng and Lu 2008). PLS models with R_p^2 of 0.66–

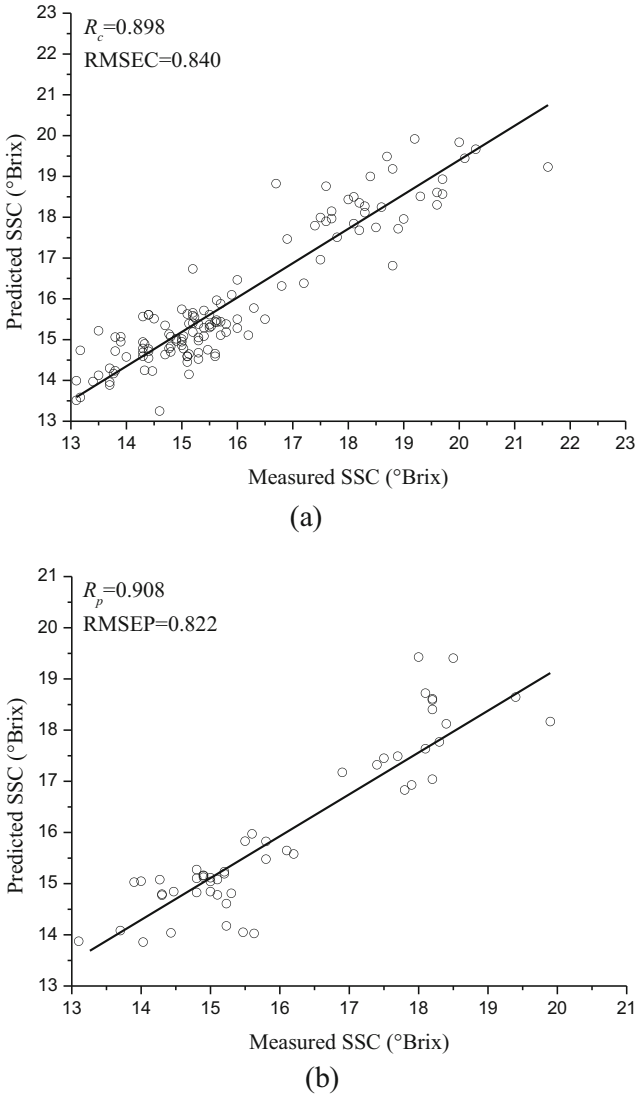

Fig. 9 Measured SSC vs. predicted values in the calibration set (**a**) and the prediction set (**b**) by the ELM-UVE-PLS model

0.88 were built for predicting SSC of 'Golden Delicious', 'Jonagold', and 'Delicious' apples (Mendoza et al. 2011), and with R_p of 0.82 and RMSEP of 0.78 for 'Golden Delicious' apples (Huang and Lu 2010).

Compared with published data on SSC prediction for apples using Vis/NIR spectroscopy and hyperspectral imaging technologies, we found that although the best predictive performances of the SSC model (R_c=0.898, R_p=0.908, RMSEC=0.840, RMSEP=0.822) established here with dielectric spectra were poorer than some reported for intact apples (Fan et al. 2009; Giovanelli et al. 2014; Moller et al. 2013; Huang et al. 2013a), they were better than some other reported values (Beghi et al. 2013; Peng and Lu 2008; Mendoza et al. 2011; Huang and Lu 2010). Furthermore, the established models to predict SSC from Vis/NIR or hyperspectral data were established with a single apple variety in these published reports, but models built from dielectric spectra data in our study involved three apple varieties. The more varieties used in modeling, the more difficult it is to improve model performance, but the models have wide range in application.

On the other hand, when compared with previous works on studying linear relationship between SSC and dielectric properties of honeydew melons (Nelson et al. 2006; Guo et al. 2008), apples (Guo et al. 2011), watermelons (Nelson et al. 2007), and peaches (Guo and Chen 2010), it was found that the nonlinear models achieved here had much better predictive performance than linear models developed earlier. Therefore, the study indicates that dielectric spectra technology may be applied to predict soluble solids content of intact apples with nonlinear models, similar to those of Vis/NIR spectroscopy and hyperspectral imaging technologies by using ANN and chemometric methods.

Conclusions

Dielectric spectroscopy combined with chemometric methods of PCA, UVE-PLS, and SPA and ANN models of GRNN, SVM, and ELM was successfully utilized for the determination of soluble solids content of three varieties of apples. Four, 29, and 11 characteristic variables were selected from original 102 variables of dielectric constants and dielectric loss factors at 51 discrete frequencies from 10 to 1800 MHz by PCA, UVE-PLS, and SPA, respectively. PCA was a more powerful data compression method than UVE-PLS and SPA, but the developed models based on PCA performed poorer than based on UVE-PLS and SPA. ELM models had less response time and better stability than GRNN and SVM models. ELM-SPA model was regarded as the best one in predicting soluble solids content of the three varieties of apples in consideration of calibration and prediction performances, stability, and response speed. The study indicates that dielectric spectra combined with artificial neural network and chemometric methods can be successfully utilized for the determination of soluble solids content of apples of several varieties. It also offers some useful technologies for developing nondestructive sensors for fruit soluble solids content based on dielectric spectra. In addition, in the future, more samples and other characteristic variable selection methods and modeling methods may need to be involved to further assess whether the ELM-SPA model is really better than other models for prediction of soluble solids content of multiple varieties of apples.

Acknowledgment This research was supported by a grant from the National Natural Science Foundation of China (project no. 31171720).

References

Beghi, R., Spinardi, A., Bodria, L., Mignani, I., & Guidetti, R. (2013). Apples nutraceutic properties evaluation through a visible and near-infrared portable system. *Food and Bioprocess Technology, 6*(9), 2547–2554.

Burges, C. J. C. (1998). A tutorial on support vector machines for pattern recognition. *Data Mining and Knowledge Discovery, 2*(2), 121–167.

Cao, J. W., Lin, Z. P., & Huang, G. B. (2012). Self-adaptive evolutionary extreme learning machine. *Neural Processing Letters, 36*(3), 285–305.

Centner, V., Massart, D. L., deNoord, O. E., deJong, S., Vandeginste, B. M., & Sterna, C. (1996). Elimination of uninformative variables for multivariate calibration. *Analytical Chemistry, 68*(21), 3851–3858.

Chang, C. C., & Lin, C. J. (2011). LIBSVM: a library for support vector machines. *ACM Transactions on Intelligent Systems and Technology, 2*(3), 27:1–27:27.

Chen, Q. S., Ding, J., Cai, J. R., & Zhao, J. W. (2012). Rapid measurement of total acid content (TAC) in vinegar using near infrared spectroscopy based on efficient variables selection algorithm and nonlinear regression tools. *Food Chemistry, 135*(2), 590–595.

Cheng, P. Y., Fan, W. L., & Xu, Y. (2013). Quality grade discrimination of Chinese strong aroma type liquors using mass spectrometry and multivariate analysis. *Food Research International, 54*(2), 1753–1760.

Cherkassky, V., & Ma, Y. Q. (2004). Practical selection of SVM parameters and noise estimation for SVM regression. *Neural Networks, 17*(1), 113–126.

Collobert, R., & Bengio, S. (2001). SVMTorch: support vector machines for large-scale regression problems. *Journal of Machine Learning Research, 1*(2), 143–160.

Deng, S. G., Xu, Y. F., Li, L., Li, X. L., & He, Y. (2013). A feature-selection algorithm based on support vector machine-multiclass for hyperspectral visible spectral analysis. *Journal of Food Engineering, 119*(1), 159–166.

Fan, G. Q., Zha, J. W., Du, R., & Gao, L. (2009). Determination of soluble solids and firmness of apples by Vis/NIR transmittance. *Journal of Food Engineering, 93*(4), 416–420.

Feng, H., Tang, J., & Cavalieri, R. P. (2002). Dielectric properties of dehydrated apples as affected by moisture and temperature. *Transactions of ASAE, 45*(1), 129–135.

Furey, T. S., Cristianini, N., Duffy, N., Bednarski, D. W., Schummer, M., & Haussler, D. (2000). Support vector machine classification and validation of cancer tissue samples using microarray expression data. *Bioinformatics, 16*(10), 906–914.

Galvao, R. K. H., Araujo, M. C. U., Jose, G. E., Pontes, M. J. C., Silva, E. C., & Saldanha, T. C. B. (2005). A method for calibration and validation subset partitioning. *Talanta, 67*(4), 736–740.

Ghiasabadi, A., Noorossana, R., & Saghaei, A. (2013). Identifying change point of a non-random pattern on (X) over-bar control chart using artificial neural networks. *International Journal of Advanced Manufacturing Technology, 67*(5–8), 1623–1630.

Giovanelli, G., Sinelli, N., Beghi, R., Guidetti, R., & Casiraghi, E. (2014). NIR spectroscopy for the optimization of postharvest apple management. *Postharvest Biology and Technology, 87*(18), 13–20.

Guo, W., & Chen, K. (2010). Relationship between dielectric properties from 10 to 4500 MHz and internal quality of peaches. *Transactions of the Chinese Society for Agricultural Machinery, 41*(3), 134–138 (in Chinese with English abstract).

Guo, W., Nelson, S. O., Trabelsi, S., & Kays, S. J. (2007a). Dielectric properties of honeydew melons and correlation with quality. *Journal of Microwave Power and Electromagnetic Energy, 41*(2), 44–54.

Guo, W. C., Nelson, S. O., Trabelsi, S., & Kays, S. J. (2007b). 10–1800 MHz dielectric properties of fresh apples during storage. *Journal of Food Engineering, 83*(4), 562–569.

Guo, W., Nelson, S. O., Trabelsi, S., & Kays, S. J. (2008). Radio Frequency (RF) dielectric properties of honeydew melon and watermelon juice and correlations with sugar content. *Transactions of the Chinese Society of Agricultural Engineering, 24*(5), 289–292 (in Chinese with English abstract).

Guo, W., Zhu, X., Nelson, S. O., Yue, R., Liu, H., & Liu, Y. (2011). Maturity effects on dielectric properties of apples from 10 to 4500 MHz. *LWT—Food Science and Technology, 44*(1), 224–230.

Huang, M., & Lu, R. (2010). Optimal wavelength selection for hyperspectral scattering prediction of apple firmness and soluble solids content. *Transactions of the ASABE, 53*(4), 1175–1182.

Huang, G. B., Zhu, Q. Y., & Siew, C. K. (2006). Extreme learning machine: theory and applications. *Neurocomputing, 70*(1–3), 489–501.

Huang, W. Q., Li, J. B., Chen, L. P., & Guo, Z. M. (2013a). Effectively predicting soluble solids content in apple based on hyperspectral imaging. *Spectroscopy and Spectral Analysis, 33*(10), 2843–2846 (in Chinese with English abstract).

Huang, Y. M., Liu, L. J., Shi, D. P., Wu, S. S., Zheng, S. Y., Fang, L., et al. (2013b). Giant dielectric permittivity and non-linear electrical behavior in $CaCu_3Ti_4O_{12}$ varistors from the molten-salt synthesized powder. *Ceramics International, 39*(6), 6063–6068.

Huang, Z. R., Sha, S., Rong, Z. Q., Chen, J. H., He, Q. L., Khan, D. M., et al. (2013c). Feasibility study of near infrared spectroscopy with variable selection for non-destructive determination of quality parameters in shell-intact cottonseed. *Industrial Crops and Products, 43*, 654–660.

Jiang, H., & Zhu, W. X. (2013). Determination of pear internal quality attributes by Fourier transform near infrared (FT-NIR) spectroscopy and multivariate analysis. *Food Analytical Methods, 6*(2), 569–577.

Jie, D. F., Xie, L. J., Fu, X. P., Rao, X. Q., & Ying, Y. B. (2013). Variable selection for partial least squares analysis of soluble solids content in watermelon using near-infrared diffuse transmission technique. *Journal of Food Engineering, 118*(4), 387–392.

Li, J. B., Huang, W. Q., Zhao, C. J., & Zhang, B. H. (2013). A comparative study for the quantitative determination of soluble solids content, pH and firmness of pears by Vis/NIR spectroscopy. *Journal of Food Engineering, 116*(2), 324–332.

Liu, H. C., & Li, S. T. (2013). Decision fusion of sparse representation and support vector machine for SAR image target recognition. *Neurocomputing, 113*, 97–104.

Liu, N., & Wang, H. (2013). Evolutionary extreme learning machine and its application to image analysis. *Journal of Signal Processing Systems for Signal Image and Video Technology, 73*(1), 73–81.

Liu, Y. D., Sun, X. D., & Ouyang, A. G. (2010). Nondestructive measurement of soluble solid content of navel orange fruit by visible-NIR spectrometric technique with PLSR and PCA-BPNN. *LWT—Food Science and Technology, 43*(4), 602–607.

Liu, Y. D., Gao, R. J., Hao, Y., Sun, X. D., & Ouyang, A. G. (2012). Improvement of near-infrared spectral calibration models for brix prediction in 'Gannan' navel oranges by a portable near-infrared device. *Food and Bioprocess Technology, 5*(3), 1106–1112.

Luczycka, D., Czubaszek, A., Fujarczuk, M., & Pruski, K. (2013). Dielectric properties of wheat flour mixed with oat meal. *International Agrophysics, 27*(2), 175–180.

Masood, I., & Hassan, A. (2013). Pattern recognition for bivariate process mean shifts using feature-based artificial neural network. *International Journal of Advanced Manufacturing Technology, 66*(9–12), 1201–1218.

Mendoza, F., Lu, R. F., Ariana, D., Cen, H. Y., & Bailey, B. (2011). Integrated spectral and image analysis of hyperspectral scattering

data for prediction of apple fruit firmness and soluble solids content. *Postharvest Biology and Technology, 62*(2), 149–160.

Moller, S. M., Travers, S., Bertram, H. C., & Bertelsen, M. G. (2013). Prediction of postharvest dry matter, soluble solids content, firmness and acidity in apples (cv. Elshof) using NMR and NIR spectroscopy: a comparative study. *European Food Research and Technology, 237*(6), 1021–1024.

Nashat, S., & Abdullah, M. Z. (2010). Multi-class colour inspection of baked foods featuring support vector machine and Wilk's λ analysis. *Journal of Food Engineering, 101*(4), 370–380.

Nelson, S. O., Soderholm, L. H., & Yung, F. D. (1953). Determining the dielectric properties of grain. *Agricultural Engineering, 34*(9), 608–610.

Nelson, S. O., Trabelsi, S., & Kays, S. J. (2006). Dielectric spectroscopy of honeydew melons from 10 MHz to 1.8 GHz for quality sensing. *Transactions of the ASABE, 49*(6), 1977–1981.

Nelson, S. O., Guo, W., Trabelsi, S., & Kays, S. J. (2007). Dielectric properties of watermelons for quality sensing. *Measurement Science & Technology, 18*, 1887–1892.

Peng, Y. K., & Lu, R. F. (2008). Analysis of spatially resolved hyperspectral scattering images for assessing apple fruit firmness and soluble solids content. *Postharvest Biology and Technology, 48*(1), 52–62.

Pontes, M. J. C., Galvao, R. K. H., Araujo, M. C. U., Nogueira, P., Moreira, T., Neto, O. D. P., et al. (2005). The successive projections algorithm for spectral variable selection in classification problems. *Chemometrics and Intelligent Laboratory Systems, 78*(1–2), 11–18.

Qian, Y. R., Wang, J., Jeon, G. G., & Jeong, J. C. (2013). Image deinterlacing using region-based back propagation artificial neural network. *Optical Engineering, 52*(7), 073107–073107.

Specht, D. F. (1991). A general regression neural network. *IEEE Transactions on Neural Networks, 2*(6), 568–576.

Wold, S., Sjostrom, M., & Eriksson, L. (2001). PLS-regression: a basic tool of chemometrics. *Chemometrics and Intelligent Laboratory Systems, 58*(2), 109–130.

Wu, D., Nie, P. C., He, Y., Wang, Z. P., & Wu, H. X. (2013). Spectral multivariable selection and calibration in visible-shortwave near-infrared spectroscopy for non-destructive protein assessment of spirulina microalga powder. *International Journal of Food Properties, 16*(5), 1002–1015.

Ye, S. F., Wang, D., & Min, S. G. (2008). Successive projections algorithm combined with uninformative variable elimination for spectral variable selection. *Chemometrics and Intelligent Laboratory Systems, 91*(2), 194–199.

Zhan, X. R., Zhu, X. R., Shi, X. Y., Zhang, Z. Y., & Qiao, Y. J. (2009). Determination of hesperidin in tangerine leaf by near-infrared spectroscopy with SPXY algorithm for sample subset partitioning and Monte Carlo cross validation. *Spectroscopy and Spectral Analysis, 29*(4), 964–968 (in Chinese with English abstract).

Zhang, J., Rivard, B., & Rogge, D. M. (2008). The successive projection algorithm (SPA), an algorithm with a spatial constraint for the automatic search of endmembers in hyperspectral data. *Sensors, 8*(2), 1321–1342.

Zhang, S. J., Zhang, H. H., Zhao, Y. R., Guo, W., & Zhao, H. M. (2013a). A simple identification model for subtle bruises on the fresh jujube based on NIR spectroscopy. *Mathematical and Computer Modelling, 58*(3–4), 545–550.

Zhang, Z. Y., Wang, Y., & Wang, K. S. (2013b). Intelligent fault diagnosis and prognosis approach for rotating machinery integrating wavelet transform, principal component analysis, and artificial neural networks. *International Journal of Advanced Manufacturing Technology, 68*(1–4), 763–773.

Zhu, Q. Y., Qin, A. K., Suganthan, P. N., & Huang, G. B. (2005). Evolutionary extreme learning machine. *Pattern Recognition, 38*(10), 1759–1763.

Zhu, F. T., Deng, Z. M., & Zhang, J. F. (2013). An integrated approach for structural damage identification using wavelet neuro-fuzzy model. *Expert Systems with Applications, 40*(18), 7415–7427.